Chapter 2
Theoretical Foundation of Low-Frequency Oscillations

In this chapter, the theoretical foundation of low-frequency oscillation (LFO) is introduced. With the increasing utilizations of measurement devices throughout the system, especially the construction of WAMS, the methods which are based on the measured data on-time or off-time have been paid more attention in last few years. First, the basic principles and research techniques of LFO are introduced. Then two kinds of methods based on system model and measured information are presented in detail, such as the eigenvalue method, the discrete Fourier transform (DFT), Hilbert–Huang transform (HHT), and so on.

2.1 The Basic Principles of Low-Frequency Oscillation

From the practical operation of power system, the reasons which may trigger the LFO phenomenon are summarized as follows: the chain structure of transmission system; the weak connection and power imbalance among different areas; shortage reserve capacity; and interactions of different control devices.

Based on the existing publications, the negative damping theory, resonance mechanism, and nonlinear theory have been proposed to explain the principles of LFOs: (1) negative damping theory is based on the linear theory and it has been widely accepted by the community. The regulations of excitation system on the generator can produce the additional negative damping. It may offset the positive damping of generator. Then, the total damping ratio is nearly to zero or even negative. Under this condition, the oscillation would be gradually amplified and cause the out of step of the generators if the system is disturbed by a small disturbance. Improving the damping by compensating the phase is the basic design idea of the LFO controller [1, 2]; (2) in some actual power systems, not all the LFO phenomena can be interpreted by the negative damping theory. Many researchers have pointed out that constant amplitude power oscillation will occur when the disturbance frequency of prime mover power is nearly to the natural frequency of power system, even if the damping is strong enough [3]. In [4], it proposed an

Y. Li et al., *Interconnected Power Systems*, Power Systems,
DOI 10.1007/978-3-662-48627-6_2

identification method to locate disturbance source by the energy conversion principles based on the comparison of negative damping theory and forced mechanism; (3) the nonlinear mechanism means that the stable structure of power system can produce nonlinear and irregular oscillations when the parameters and disturbance are in the special range [5, 6]. It has big difference from the linear theory. However, this principle still stays in the period of theoretical study because of the limitation of mathematical tool. It should be noted that the principle of LFO in this paper is based on the negative damping theory.

Up to now, there are many different classification methods according to different criteria. Usually, LFO belongs to the branch of rotor angle stability. According to widely accepted results, the classification of LFO is divided into two forms: one is the local oscillation mode; the other is the inter-area oscillation mode [1, 7].

2.1.1 Local Mode

Local oscillation mode involves in the oscillation between the single generator or a group of generators and the rest of generators in the local area. In general, the oscillation frequency of this mode is in the range of 1–2.5 Hz. Due to this definition, it can be concluded that the influence of the local mode is just in the specific area and it can be controlled expediently by the PSS [1].

To investigate the physical nature of low-frequency electromechanical power oscillations in the time domain, a model of a typical two-area power system was created. This two-area system was created by Ontario Hydro for a research report commissioned by the Canadian Electrical Association [8, 9]. This system was designed to exhibit the different types of oscillations that occur in an interconnected system [8, 9]. This two-area system can be considered as a useful tool for the study of the electromechanical oscillations in the GB power system. For this purpose Area 1 represents the Scottish power system and Area 2 represents the English power system. A single line diagram of the two-area system is shown in Fig. 2.1.

This simple model shows the electromechanical oscillations that are inherent in the two-area system. There are three possible electromechanical modes of oscillations in this system. There are two local modes, one in which generator 1 swings

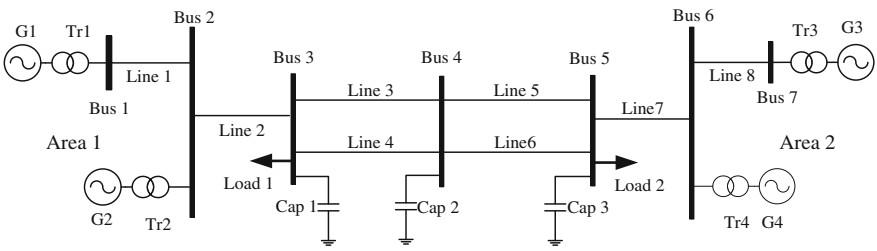

Fig. 2.1 A typical two-area system

against generator 2, and another in which generator 3 swings against generator 4. In addition, there is also one inter-area mode, in which the generators in Area 1 swing against the generators in Area 2. In this section, nonlinear simulations will be used to give an insight into the nature of these different types of electromechanical oscillations. In these nonlinear simulations, the different modes of oscillation are initiated using a range of different disturbances.

To investigate the nature of the local mode in Area 1, changes in the mechanical torque of the generators in that area were simulated. To properly investigate the behavior of the local mode in Area 1 it is important to minimize the excitation of the inter-area mode during these simulations. To achieve this goal, equal and opposite step changes in the mechanical torque of the two generators in Area 1 were simulated simultaneously. For example, a change of −0.01 p.u. in the mechanical torque of generator 1 is simulated, and then a corresponding change of 0.01 p.u. is made in the mechanical torque of generator 2. The response of the generators, in terms of speed, to this pair of small disturbances in Area 1 is presented in Fig. 2.2.

In Area 1, the rotor speed changes of generator 1 and 2 were in anti-phase, i.e, generator 1 oscillated against generator 2 in the local mode. This local mode dominated the oscillation for approximately 7 s, at which time the generators began to swing together in the inter-area mode. The generators in Area 2 experienced oscillations with lower amplitude than those seen in Area 1. These oscillations were in phase with one another and are driven by the inter-area mode, the local mode in Area 2 was not observed here. These simulation results show that the frequency of the local oscillation mode in Area 1 is approximately 1 Hz.

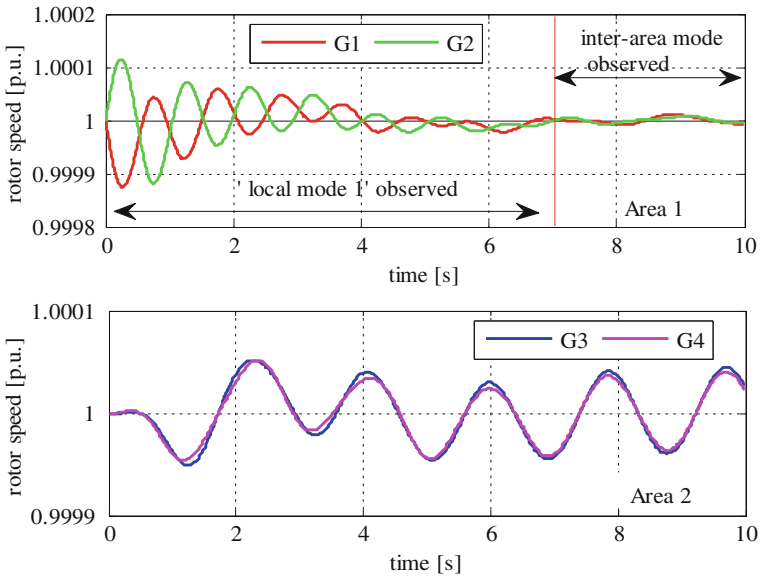

Fig. 2.2 Generator rotor speed responses to the disturbances occurred in Area 1

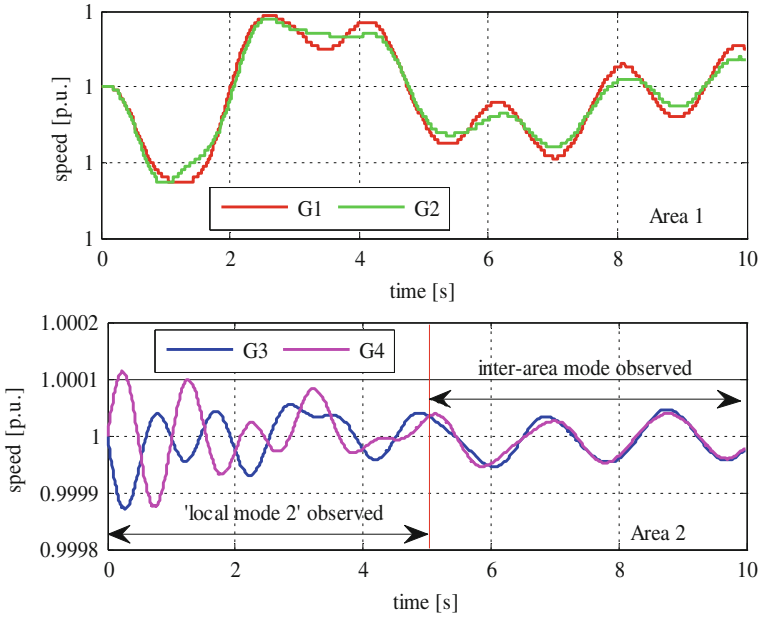

Fig. 2.3 Generator rotor speed responses to the disturbances occurred in Area 2

The same method used to excite the local mode in Area 1 is used to excite the local mode in Area 2. An equal and opposite step change of the mechanical torque of the generators in Area 2 was simulated. The change in the mechanical torque of generator 3 was −0.01 p.u. and the change in the mechanical torque of generator 4 was 0.01 p.u. The generator rotor speed responses to the small disturbances that occurred in Area 2 are shown in Fig. 2.3.

For a small disturbance in Area 2, generator 3 immediately began to swing against generator 4; this local mode dominated the response for about 5 s, after which time the inter-area oscillatory mode began to dominate. The generators in Area 1 were driven by the inter-area mode and moved together with oscillations of much lower amplitude than those seen in Area 2. The frequency of the local mode in Area 2 was approximately 1 Hz.

2.1.2 Inter-Area Mode

Inter-area oscillation mode represents one part of generators swinging against the other part of generators in wide-area systems. Because the equivalent generator in different areas has bigger constant of inertia, the oscillation frequency of this mode is smaller than the local mode and the frequency range is about 0.1–1 Hz. Compared with the local mode, the inter-area mode has some special

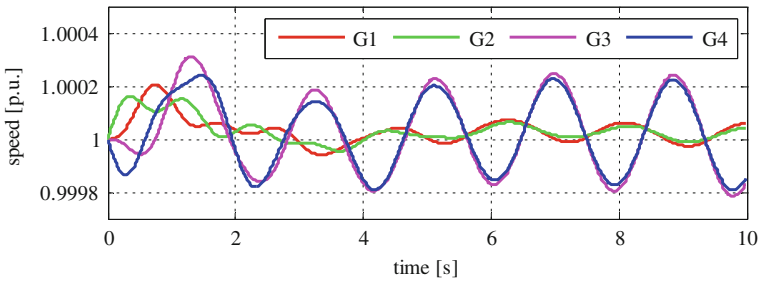

Fig. 2.4 Generator rotor speed oscillations dominated by inter-area mode

characteristics: the lasting time is longer, the impact is more slowly and widely, the damping value is smaller, and it is more difficult to be controlled [1].

The inter-area mode can be directly provoked by changing the mechanical torque of one generator in each of the different areas. In this case, the mechanical torque of generator 2 was increased by 0.01 p.u., while the mechanical torque of generator 4 was reduced by 0.01 p.u. The generator speed responses to these small disturbances are shown in Fig. 2.4.

As Fig. 2.4 presents, the inter-area mode dominated the response of the generator rotor speeds to these disturbances. The generators in Area 1 began to swing against the generators in Area 2 immediately after the disturbances, and the magnitudes of the speed change of the generators in Area 2 were larger than the magnitudes of the speed change of the generators in Area 1. Initially, the oscillations in Area 1 were strongly influenced by the local mode. This is evident as for the first 4 s the generators in Area 1 oscillated against one another while also moving together in the inter-area mode. The frequency of the inter-area mode was approximately 0.5 Hz. The inter-area mode was not damped by any external control and the amplitude of the inter-area oscillation was seen to increase.

For obtaining more information about inter-area oscillations, the responses of the system frequency and the inter-area active power flow to the disturbances were analyzed. Figure 2.5 presents the system frequency response to the disturbances measured in Area 1 (bus 3) and Area 2 (bus 5). The oscillations in the frequency deviation in Area 1 were approximately in anti-phase to the oscillations in the frequency deviation in Area 2, which is consistent with the changes seen in the generator rotor speeds in Fig. 2.4.

Figure 2.6 shows the active power flow over line 3 after the disturbances. The oscillatory power flow on line 3 is purely driven by the inter-area mode, with no influence from the local modes. This occurs because the physical mechanism behind electromechanical oscillations is the active power exchange between the generators that are involved in the oscillatory mode. Therefore, as line 3, like all of the inter-tie lines, only carries power between the two areas, then only the inter-area oscillations, and not the local mode oscillations, will be seen on these lines.

The power exchange driving the local modes in Areas 1 and 2 occurs along lines 1 and 8, respectively. Therefore, the power flow associated with these local

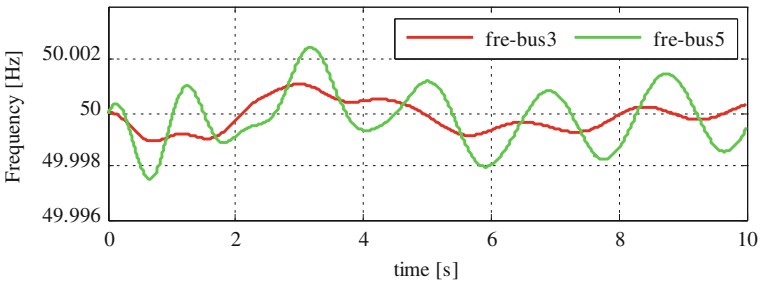

Fig. 2.5 System frequency responses in inter-area mode

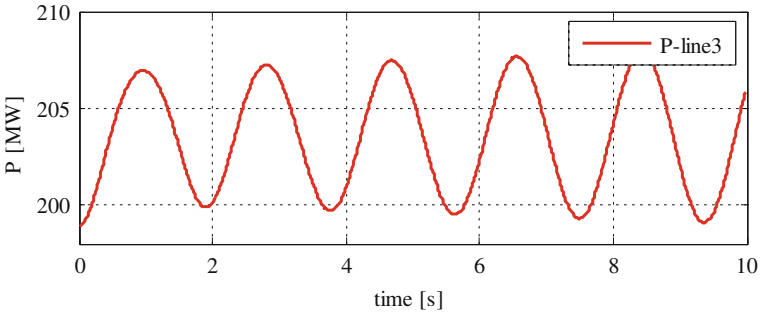

Fig. 2.6 Oscillatory active power flow on transmission line 3

oscillation modes will only be seen on these lines. To demonstrate this, the power flow on line 1 during the disturbances is shown in Fig. 2.7. The variation of the power flow on line 1 shows the difference between the power flow that supports the local mode and the power flow that supports the inter-area mode. This can be seen by comparing the power flow during the first four seconds after the disturbances, where the local mode dominates, with the power flow during the next six seconds, where the inter-area mode dominates.

To further examine the characteristics of the inter-area oscillations, a three-phase short-circuit fault was simulated on bus 4, the mid-point of the inter-area lines that connect the two areas. A short circuit represents a much larger disturbance to the system than the small mechanical power changes simulated in the previous sections and as such will offer greater insight into the behavior of the oscillatory modes. The transient fault occurred at 0.1 s and was cleared after at 0.2 s. The response of the rotor speed of each generator to the disturbance is presented in Fig. 2.8, and the active power transfer over one of the inter-tie line (line 3) is shown in Fig. 2.9.

As seen from Figs. 2.8 and 2.9, after the system recovered from the transient fault, the generators in Area 1 started to oscillate against the generators in Area 2 in inter-area mode around the new system equilibrium point. The inter-area mode was clearly visible in the generator rotor speed responses and the oscillatory active power flow on the inter-tie line.

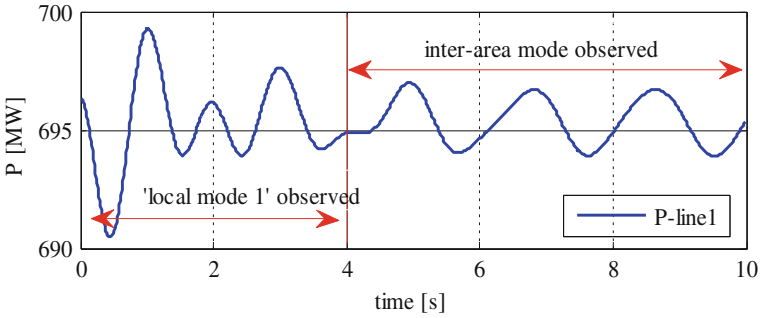

Fig. 2.7 Oscillatory active power flow on transmission line 1

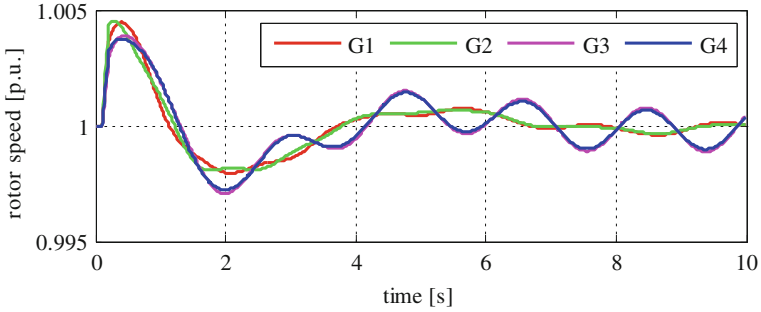

Fig. 2.8 Responses of the generator rotor speeds to the large disturbance

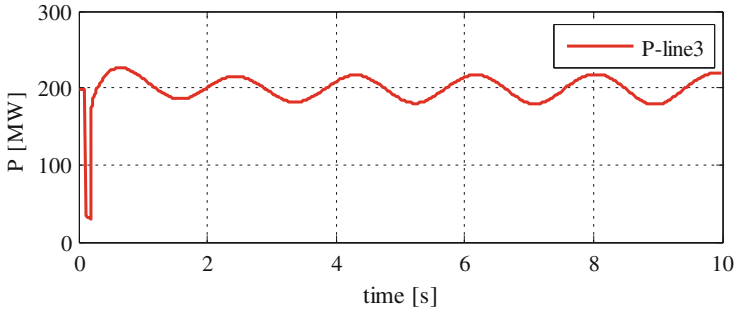

Fig. 2.9 Active power transfer over the tie line after the disturbance

2.2 Techniques Based on System Model

In Sect. 2.1, a number of nonlinear simulations were performed to show the physical nature behind power system oscillations. In the nonlinear simulations the transients were induced using small disturbances (e.g., a 1 % change of mechanical

torque), and the system responses were essentially linear. Although the initial system response to the three-phase transient fault was nonlinear, the response quickly settled into post-fault oscillations that are essentially linear around the post-fault equilibrium point. This means that, for a study of electromechanical oscillations, the system model can be linearized around the steady-state point. The linearization of the system model provides an excellent opportunity for modal analysis [8]. Modal analysis can be used to perform a wide range of tasks, such as determining the oscillatory modes, the sources of the oscillatory modes, and the parameters needed for designing oscillation controllers.

In this section, the modal analysis methods will be introduced. This analysis tool will then be used to explain the physical phenomenon of inter-area oscillations presented in the Sect. 2.1. Generally speaking, this method based on the system model or device parameters can be classified into two kinds: one is the linear methods, such as the eigenvalue analysis; the other is nonlinear methods, for example, time-domain simulation and normal form analysis.

2.2.1 Linearization of the State Equation

If there are a set of state variables x_0 and a set of inputs u_0 with which all the derivatives $\dot{x}_1, \dot{x}_2, \cdots, \dot{x}_n$ are simultaneously zero, as represented by the (2.1), we can say that the system is at a steady state [10].

$$\dot{x}_0 = f(x_0, u_0) \tag{2.1}$$

If a stable system is disturbed from steady state by a small disturbance, i.e., Δx and Δu, it will eventually come to rest at a new steady state. This transition will still satisfy (2.1), and hence we have

$$\dot{x} = f[(x_0 + \Delta x), (u_0 + \Delta u)] \tag{2.2}$$

As the disturbance is assumed to be very small, the nonlinear equation $f(x, u)$ can be approximated using a Taylor series expansion in terms of Δx and Δu. If we only consider the first-order terms of this expansion we will have

$$\begin{aligned} \dot{x}_i &= \dot{x}_{i0} + \Delta\dot{x}_i = f_i[(x_0 + \Delta x), (u_0 + \Delta u)] \\ &= f_i(x_0, u_0) + \frac{\partial f_i}{\partial x_1}\Delta x_1 + \cdots + \frac{\partial f_i}{\partial x_n}\Delta x_n + \frac{\partial f_i}{\partial u_1}\Delta u_1 + \cdots + \frac{\partial f_i}{\partial u_r}\Delta u_r \end{aligned} \tag{2.3}$$

Since $\dot{x}_{i0} = f_i(x_0, u_0)$,we have

$$\Delta\dot{x}_i = \frac{\partial f_i}{\partial x_1}\Delta x_1 + \cdots + \frac{\partial f_i}{\partial x_n}\Delta x_n + \frac{\partial f_i}{\partial u_1}\Delta u_1 + \cdots + \frac{\partial f_i}{\partial u_r}\Delta u_r, \quad i = 1, 2, \ldots, n \tag{2.4}$$

in the same way based on (2.2), we have

$$\Delta y_i = \frac{\partial g_i}{\partial x_1}\Delta x_1 + \cdots + \frac{\partial g_i}{\partial x_n}\Delta x_n + \frac{\partial g_i}{\partial u_1}\Delta u_1 + \cdots + \frac{\partial g_i}{\partial u_r}\Delta u_r, \quad j = 1, 2, \ldots, m \tag{2.5}$$

Therefore, the linearized system state equations around the equilibrium point are given as [10]

$$\Delta \dot{x} = A\Delta x + B\Delta u \tag{2.6}$$

$$\Delta y = C\Delta x + D\Delta u \tag{2.7}$$

with

$$A = \begin{bmatrix} \frac{\partial f_1}{\partial x_1} & \cdots & \frac{\partial f_1}{\partial x_n} \\ \vdots & \vdots & \vdots \\ \frac{\partial f_n}{\partial x_1} & \cdots & \frac{\partial f_n}{\partial x_n} \end{bmatrix}, \quad B = \begin{bmatrix} \frac{\partial f_1}{\partial u_1} & \cdots & \frac{\partial f_1}{\partial u_r} \\ \vdots & \vdots & \vdots \\ \frac{\partial f_n}{\partial u_1} & \cdots & \frac{\partial f_n}{\partial u_r} \end{bmatrix},$$

$$C = \begin{bmatrix} \frac{\partial g_1}{\partial x_1} & \cdots & \frac{\partial g_1}{\partial x_n} \\ \vdots & \vdots & \vdots \\ \frac{\partial g_m}{\partial x_1} & \cdots & \frac{\partial g_m}{\partial x_n} \end{bmatrix}, \quad D = \begin{bmatrix} \frac{\partial g_1}{\partial u_1} & \cdots & \frac{\partial g_1}{\partial u_r} \\ \vdots & \vdots & \vdots \\ \frac{\partial g_m}{\partial u_1} & \cdots & \frac{\partial g_m}{\partial u_r} \end{bmatrix}.$$

where Δx is the state vector of length n; Δu is input disturbance vector of length r; Δy is the output vector of length m; A is the state matrix of size $n \times n$; B is the input matrix of size $n \times r$; C is the output matrix of size $m \times n$; and D is a matrix of size $m \times r$, which defines the proportion of the input which directly influences the output, Δy.

2.2.2 Calculation of Eigenvalues and Eigenvectors

The following equation is defined as the characteristic equation of matrix A [10]:

$$\det(\lambda I - A) = 0 \tag{2.8}$$

The n solutions of the characteristic equation $\lambda = [\lambda_1, \lambda_2, \ldots, \lambda_n]$ are the eigenvalues of A. The eigenvalues may be real or complex. If matrix A is real, then the complex eigenvalues occur in conjugate pairs.

For any eigenvalue λ_i, a n-column vector φ_i satisfied

$$A\varphi_i = \lambda_i \varphi_i \quad i = 1, 2, \ldots, n \tag{2.9}$$

is the right eigenvector of the A matrix associated with the eigenvalue λ_i. The right eigenvector ϕ_i has the form

$$\varphi_i = \begin{bmatrix} \varphi_{1i} \\ \varphi_{2i} \\ \cdots \\ \varphi_{ni} \end{bmatrix} \tag{2.10}$$

The right eigenvector describes how each mode of oscillation is distributed among the system states. In other words, it indicates on which system variables the mode is more observable [11]. The magnitudes of the elements of φ_i give the extent of the behaviors of the n state variables in the ith mode, and the angles of elements give the phase displacements of the state variables with regard to the mode. Thus, the right eigenvector is called mode shape.

Similarly, if a n-row vector φ_i satisfies

$$\psi_i A = \lambda_i \psi_i \quad i = 1, 2, \ldots, n \tag{2.11}$$

it is called the left eigenvector of the A matrix associated with the eigenvalue λ_i. The left eigenvector has the form

$$\psi_i = [\psi_{i1}\ \psi_{i2} \ldots \psi_{in}] \tag{2.12}$$

The left eigenvector ψ_i can be used to identify which combination of state variables displays only the ith mode. Thus, the kth element of the right eigenvector φ_i measures the activity of the variable x_k in the ith mode, and the kth element of the left eigenvector ψ_i weights the contribution of this activity to the ith mode.

2.2.3 Determination of Oscillation Parameters

The damping ratio ξ determines the decaying rate of the amplitude of an oscillation. The eigenvalues λ of A matrices can be obtained by solving the root of the characteristic equation. For a complex–conjugate pair of eigenvalues

$$\lambda = \sigma \pm j\omega \tag{2.13}$$

the corresponding damping ratio and oscillation frequency f can be defined as follows:

$$\xi = \frac{-\sigma}{\sqrt{\sigma^2 + \omega^2}} \tag{2.14}$$

$$f = -\frac{\omega}{2\pi} \tag{2.15}$$

If λ_i is an eigenvalue of A, v_i and w_i are nonzero column and row vectors, respectively, such that the following relations hold:

$$Av_i = \lambda_i v_i \quad i = 1, 2, \ldots, n \tag{2.16}$$

$$w_i A = \lambda_i w_i \quad i = 1, 2, \ldots, n \tag{2.17}$$

where the vectors v_i and w_i are known as the right and left eigenvectors of matrix A. And they are henceforth considered normalized such that

$$w_i \cdot v_i = 1 \tag{2.18}$$

Then the participation factor P_{ki} (the kth state variable x_k in the ith eigenvalue λ_i) can be given as

$$P_{ki} = |v_{ki}||w_{ki}| \tag{2.19}$$

where w_{ki} and v_{ki} are the ith elements of w_k and v_k, respectively.

2.2.4 Brief Summary of System Model Analysis Techniques

Model-based method has been widely utilized to extract the modal information as well as to identify the transfer function and to design the controller. Generally speaking, this method based on the system model or device parameters can be classified into two kinds: one is the linear methods, such as the eigenvalue analysis; the other is nonlinear methods, for example, time-domain simulation and normal form analysis. The advantages of these approaches are that they allow the investigation of the dynamic behavior of the system under different modes and all the characteristic patterns leading to complicated phenomena can be detected. Moreover, the nonlinear behaviors of other controllers are also taken into account simultaneously. However, there are also many limitations for the application of the time-domain simulation: (1) it is impossible to trigger all the oscillation modes because the disturbance location and style are chosen specifically; (2) it is difficult to determine the oscillation characteristics only based on the limited time-domain responses; (3) time-domain simulation model is based on the detailed parameters of all elements, and it is impossible to get these parameters accurately because of the benefits of manufacturers; and (4) longer simulation time and heavy computation load do not make it fulfill the requirements of online application. According to the features of eigenvalue analysis and time-domain simulation, both methods should be utilized mutually and in a complementary manner.

2.3 Techniques Based on Measured Information

A large collection of methods has been investigated for extracting model information from measured system responses. In this section, these methods are divided into two groups according to the number of disposed signals. The first kind of approach is presented to calculate the oscillatory parameters of single measured signal, such as discrete Fourier transform (DFT), Hilbert–Huang transform (HHT), wavelet transform (WT), and so on. The second kind of method is presented to extract the dynamic oscillation characteristic based on the ensemble measurement matrix, such as Prony method, multi-Prony technique, and so on.

2.3.1 Discrete Fourier Transform

Discrete Fourier transform (DFT) is a form of Fourier analysis that is applicable to the uniformly spaced samples taken from an input signal $x(t)$ of a continuous function. In particular, the DFT is the primary tool of digital signal processing and related fields. A key enabling factor for its widely applications is the fact that the DFT can be computed efficiently in practice using a fast Fourier transform (FFT) algorithm. The FFT is calculated at discrete steps in the frequency domain, just as the input signal is sampled at discrete instants in the time domain [12].

Consider the process of selecting N samples: $x(k\Delta T)$ with $\{k = 0, 1, \ldots, N-1\}$, ΔT being the sampling interval. This is equivalent to multiplying the sampled data train by a "windowing function" $\omega(t)$, which is a rectangular function of time with unit magnitude and a span of $N\Delta T$. With the choice of samples ranging from 0 to $N-1$, the windowing function can be viewed as starting at $-\Delta T/2$ and ending at $(N-1/2)\Delta T$.

The collection of signal samples fall in the data window: $x(k\Delta T)$ with $\{k = 0, 1, \ldots, N-1\}$. These samples can be viewed as being obtained by the multiplication as follows:

$$y(t) = x(t)\omega(t)\delta(t) = \sum_{k=0}^{N-1} x(k\Delta T)\delta(t - k\Delta T) \tag{2.20}$$

The convolution of FFTs of the three functions finally get the FFT of the sampled windowed function $y(t)$.

In order to obtain the DFT of $y(t)$, the FFT of $y(t)$ is to be sampled in the frequency domain. The discrete steps in the frequency domain are multiples of $1/T_0$, where T_0 is the span of the windowing function. The frequency sampling function $\Phi(f)$ is given by

$$\Phi(f) = \sum_{n=-\infty}^{\infty} \delta\left(f - \frac{n}{T_0}\right) \tag{2.21}$$

and its inverse FFT is

$$\Phi(t) = T_0 \sum_{n=-\infty}^{\infty} \delta(t - nT_0) \tag{2.22}$$

It is essential to multiply the FFT $Y(f)$ with $F(f)$ to obtain the samples in the frequency domain. To obtain the corresponding time-domain function $x'(t)$, a convolution in the time domain of $y(t)$ and $\Phi(t)$ will be required:

$$\begin{aligned} x'(t) = y(t)\Phi(t) &= \left[\sum_{k=0}^{N-1} x(k\Delta T)\delta(t - k\Delta T)\right]\left[T_0 \sum_{n=-\infty}^{\infty} \delta(t - nT_0)\right] \\ &= T_0 \sum_{n=-\infty}^{\infty} \left[\sum_{k=0}^{N-1} x(k\Delta T)\delta(t - k\Delta T - nT_0)\right] \end{aligned} \tag{2.23}$$

Through $N-1$ and the sampling in frequency domain, the original N samples in time domain are transformed to an infinite train of N samples with a period T_0. Note that we may still consider this function to be an approximation of $x(t)$ although the original function $x(t)$ was not periodic and the function is $x'(t)$.

The FFT of the periodic function $x'(t)$ is a sequence of impulse functions in frequency domain of the FFT. Thus

$$x'(f) = \sum_{n=-\infty}^{\infty} \alpha_n \delta\left(f - \frac{n}{T_0}\right) \tag{2.24}$$

with

$$\alpha_n = \frac{1}{T_n} \int_{-T_0/2}^{T_0/2} x'(t) \mathrm{e}^{-\frac{j2\pi n}{T_0}} \mathrm{d}t, \quad n = 0, \pm 1, \pm 2 \ldots \tag{2.25}$$

Substituting for $x'(t)$ in the above expression for α_n,

$$\alpha_n = \frac{1}{T_0} \int_{-T_0/2}^{T_0/2} T_0 \sum_{m=-\infty}^{\infty} \left[\sum_{k=0}^{N-1} x(k\Delta T)\delta(t - k\Delta T - mT_0)\mathrm{e}^{-\frac{j2\pi n}{T_0}} \mathrm{d}t\right], \quad n = 0, \pm 1, \pm 2 \ldots \tag{2.26}$$

The index m designates the periodic sequences of the FFT of the windowed function. Since the limits on the integration span one period only, we may remove the summation on m, and set $m = 0$, thus using only the samples over the period. (2.22) then becomes

$$\alpha_n = \int_{-T_0/2}^{T_0/2} \sum_{k=0}^{N-1} x(k\Delta T)\delta(t - k\Delta T)\mathrm{e}^{-\frac{j2\pi n}{T_0}}\mathrm{d}t, \quad n = 0, \pm 1, \pm 2\ldots \tag{2.27}$$

or

$$\alpha_n = \sum_{k=0}^{N-1} \int_{-T_0/2}^{T_0/2} x(k\Delta T)\delta(t - k\Delta T)\mathrm{e}^{-\frac{j2\pi n}{T_0}}\mathrm{d}t = \sum_{k=0}^{N-1} x(k\Delta T)\delta(t - k\Delta T)\mathrm{e}^{-\frac{j2\pi nk\Delta T}{T_0}} \tag{2.28}$$

Since there are N samples in the data window T_0, $N\Delta T = T_0$. Therefore,

$$\alpha_n = \sum_{k=0}^{N-1} x(k\Delta T)\mathrm{e}^{-\frac{j2\pi nk}{N}} \tag{2.29}$$

with

$$n = 0, \pm 1, \pm 2\ldots$$

Note that there are only N distinct coefficients α_n although the index n goes over all positive and negative integers. Thus, α_{N+1} is the same as α_1 and the FFT $x'(f)$ has only N distinct values corresponding to frequencies $f = n/T_0$, with n ranging from 0 through $N - 1$.

2.3.2 *Prony Algorithm and Multi-Prony*

Prony method is a linear combination of complex exponential functions to describe the mathematical model of equal interval sampling data, often referred to as the Prony model, and gives the approximate solution algorithm. Prony analysis has been shown to be a feasible technique to model a linear combination of damped complex exponentials to signals that are uniformly sampled.

There are three basic steps in the Prony algorithm:

Step 1 Determine the linear prediction parameters that fit the available data.
Step 2 Solve the roots of the polynomial formed in *step 1*, and find the prediction coefficient that will yield the estimates of damping and sinusoidal frequencies of each of the exponential terms.

Step 3 With the solution obtained in *step 2*, a second linear equation will obtained.

Then, the estimate of the exponential amplitude and sinusoidal initial phase can be received. Prony algorithm and multi-Prony estimate parameters of modes associated with a signal, or certain set of signals [13], such as mode frequency, amplitude, phase, and damping ratio. The Prony method calculates or estimates a linear exponential function of the form (2.30) by approximating in the least square sense to a certain set of equally sampled discrete data.

$$\hat{y}(t) = \sum_{i=1}^{m} A_i e^{\sigma_i t} \cos(2\pi f_i t + \varphi_i) \quad \text{for } t \geq 0 \tag{2.30}$$

Equation (2.30) may be written in a complex exponential form as

$$\hat{y}(t) = \sum_{i=1}^{m} B_i e^{\lambda_i t} + B_i^* e^{\lambda_i^* t} \quad \text{for } t \geq 0 \tag{2.31}$$

where m is the number of modes, $B_i = \frac{A_i}{2} e^{j\varphi_i}$, $\lambda_i = \sigma_i + j\omega_i$ and * indicates complex conjugate. Moreover, (2.31) could be expressed in a simplified manner as

$$\hat{y}(t) = \sum_{i=1}^{p} B_i e^{\lambda_i t} \quad \text{for } t \geq 0 \tag{2.32}$$

where p is the number of the estimated eigenvalues.

Multi-Prony analysis is just a vector–matrix extension of Prony analysis, considering multiple outputs of the form $y(t) = cx(t)$ at the same time [14].

Consider also that, for (2.31) or (2.32), the B_i and the λ_i are distinct. Let $y(t)$ be N samples evenly spaced by Δt such that

$$y(t_k) = y(k) \quad \text{for } k = 0, 1, \ldots, N-1 \tag{2.33}$$

The Prony estimated output signal at time $t_k = k$ will be

$$\hat{y}(t) = \sum_{i=1}^{p} B_i e^{\lambda_i k \Delta t} \quad \text{for } k = 0, 1, \ldots, N-1 \tag{2.34}$$

For convenience, define $z_i = e^{\lambda_i \Delta t}$, then

$$\hat{y}(t) = \sum_{i=1}^{p} B_i z_i^{\mathrm{k}} \quad \text{for } k = 0, 1, \ldots, N-1 \tag{2.35}$$

As can be seen, the objective with Prony method is to find the values of B_i and z_i that produce

$$\hat{y}(k) = y(k) \quad \text{for all } k \tag{2.36}$$

Assuming that (2.36) is true for all k, set

$$\begin{aligned} y(0) &= B_1 + B_2 + \cdots + B_p \\ y(1) &= B_1 z_1 + B_2 z_2 + \cdots + B_p z_p \\ y(2) &= B_1 z_1^2 + B_2 z_2^2 + \cdots + B_p z_p^2 \\ &\vdots \qquad\qquad \vdots \\ y(N-1) &= B_1 z_1^{N-1} + B_2 z_2^{N-1} + \cdots + B_p z_p^{N-1} \end{aligned} \tag{2.37}$$

In matrix form,

$$\begin{bmatrix} y(0) \\ y(1) \\ y(2) \\ \vdots \\ y(N-1) \end{bmatrix} = \begin{bmatrix} z_1^0 & z_2^0 & \cdots & z_p^0 \\ z_1^1 & z_2^1 & \cdots & z_p^1 \\ z_1^2 & z_2^2 & \cdots & z_p^2 \\ \vdots & \vdots & \vdots & \vdots \\ z_1^{N-1} & z_2^{N-1} & \cdots & z_p^{N-1} \end{bmatrix} \begin{bmatrix} B_1 \\ B_2 \\ \\ \vdots \\ B_p \end{bmatrix} \tag{2.38}$$

Note that these equations are nonlinear in z and that we need $N \geq 2p + 1$.

The method to solve the above equations may be described as follows: Let z_i for $i = 1, 2, \ldots, p$ be the roots of some p_{th} order polynomial $\Pi(z)$:

$$\Pi(z) = (z - z_1)(z - z_2)\ldots(z - z_p) = z^p - \alpha_1 z^{p-1} - \cdots - \alpha_{p-1} z - \alpha_p = 0 \tag{2.39}$$

Now, multiply the first equation in (2.37) by $-\alpha_p$, the second equation by $-\alpha_{p-1}\ldots$, the pth equation by $-\alpha_1$, and the $(p + 1)$th equation by 1, and add the results. Then,

$$\begin{aligned} &y(p) - \alpha_1 y(p-1) - \alpha_2 y(p-2) - \cdots - \alpha_p y(0) \\ &\quad = B_1(z_1^p - \alpha_1 z_1^{p-1} - \alpha_2 z_1^{p-2} - \cdots - \alpha_p z_1^0) + B_2(z_2^p - \alpha_1 z_2^{p-1} - \alpha_2 z_2^{p-2} - \cdots - \alpha_p z_2^0) + \cdots \end{aligned} \tag{2.40}$$

Since (2.39) is true for all z_i, the right-hand members of the above equation vanish and it is obtained that

$$y(p) = \alpha_1 y(p-1) + \alpha_2 y(p-2) + \cdots + \alpha_p y(0) \tag{2.41}$$

Applying repeatedly the above process starting this time from the second equation in (2.37), and next from the third equation, and so on, the following $N-1-p$ set of linear equations can be obtained:

$$\begin{bmatrix} y(p) \\ y(p+1) \\ y(p+2) \\ \vdots \\ y(N-1) \end{bmatrix} = \begin{bmatrix} y(p-1) & y(p-2) & \cdots & y(0) \\ y(p) & y(p-1) & \cdots & y(1) \\ y(p+1) & y(p) & \cdots & y(2) \\ \vdots & \vdots & \vdots & \vdots \\ y(N-2) & y(N-3) & \cdots & y(N-p-1) \end{bmatrix} \begin{bmatrix} \alpha_1 \\ \alpha_2 \\ \vdots \\ \alpha_p \end{bmatrix} \tag{2.42}$$

This set of equations can be solved directly if $N = 2p + 1$, or approximately by least squares if $N > 2p + 1$.

Once the α's are obtained, the z_i's values could be found from (2.39). Then, (2.38) become linear with known coefficients and the B_i's may be determined. Note that B_i's have the information about amplitude and initial phase of the modes, while the z_i's content the values for σ_i and ω_i of the modes.

2.3.3 Wavelet Transform and Its Improvements

The wavelet analysis has been introduced as a windowing technique with variable-sized regions to overcome the drawback of the fixed size window [15]. It has been one of the most important and fastest evolving signal processing tools of the last twenty years. Wavelet decomposition introduces the notion of scale as an alternative to frequency and maps a signal into a timescale plane which is equivalent to the time–frequency plane used in the short time FFT. Each scale in the timescale plane corresponds to a certain range of frequencies in the time–frequency plane.

The wavelet $\psi(t)$ (or mother wavelet) is a function of zero average [16]

$$\int_{-\infty}^{\infty} \psi(t)\mathrm{d}t = 0 \tag{2.43}$$

which is dilated with a scale parameter a, and translated by b to produce the daughter wavelets:

$$\psi_{a,b}(t) = \frac{1}{\sqrt{a}}\psi\left(\frac{t-b}{a}\right) \tag{2.44}$$

Different types of wavelets are often grouped into wavelet families according to their properties. The typical wavelet families are included in the Matlab® Wavelet Toolbox™ version 4.1.

The wavelet transform of $y(t)$ at the scale a and position b is computed by correlating $y(t)$ with a wavelet function ψ:

$$Wy(a,b) = C(a,b) = \int_{-\infty}^{\infty} y(t)\frac{1}{\sqrt{a}}\psi^*\left(\frac{t-b}{a}\right)\mathrm{d}t \tag{2.45}$$

where $C(a,b)$ is the wavelet coefficient (approximately directly proportional to the amplitude of a specific mode) with the scale a (inversely proportional to the wavelet center frequency) and position b, ψ^* is the complex conjugated wavelet function. $y(t)$ denotes the original signal in continuous time t, and it can be any signal in a power system which contains the studied oscillation information. Those signals include, for example, the interconnecting line power flow between oscillating systems, the angular speed of an oscillating generator, and the voltage angle difference between oscillating systems.

The center frequency of the wavelet function f_c is defined as the frequency that maximizes the FFT of the wavelet function ψ:

$$f_c = \{f \left| \max \hat{\psi}(f) = \hat{\psi}(f_c) \right.\} \tag{2.46}$$

where f is frequency and $\hat{\psi}$ is the FFT of the wavelet function.

The wavelet center frequency changes accordingly when the wavelet scale is changed. If the scale is increased (the wavelet function is stretched), the center frequency of the wavelet function is decreased and vice versa. For example, if the wavelet function is scaled to have a center frequency of 0.3 Hz, it is referred to as "0.3 Hz wavelet."

The wavelet transform can be classified as continuous or discrete wavelet transform (DWT). In general, continuous wavelets are better for time–frequency analysis and discrete wavelets are more suitable for decomposition and compression [16].

Continuous wavelet transform (CWT) is calculated that both the parameters a and b are continuous variables in the interval of interest. In practice, both a and b are discrete when sampled data is analyzed. The wavelet transform is still referred to as continuous if a is an arbitrarily selected set of scales (selected according to frequency band in question and the needed resolution in frequency) and b is set by the signal sampling interval.

It is possible to use the DWT to reduce the amount of data produced by the wavelet transform that uses a certain subset of scales a, and positions b. The signal reconstruction will be as accurate as using CWT.

Because it can (with certain accuracy) extract the amplitudes of various frequency components of the signal along the time axis, the wavelet transform can be used in damping estimation. After that, the damping of the frequency components (modes) can be identified. The accuracy of the wavelet transform to measure time–

frequency variations of spectral components is limited by Heisenberg's uncertainty principle.

Both wavelet characteristics, time and frequency resolutions, affect the damping estimation of the mode after the wavelet transform is performed. Therefore, the mother wavelets with good enough frequency resolution are significantly to separate the modes from each other but having as good as possible time resolution also.

While damping the electromechanical oscillations, the analyzed signals always have a certain amount of measurement noise which is due to the measurement errors of the analyzed quantities (voltages, currents, and frequencies). The measurement errors are mainly caused by the inaccurate measurement of the PMUs and transformers. The ability of different mother wavelets to separate the noise from the actual mode is different but generally the wavelet transform is quite insensitive to noise in the analyzed signals.

2.3.4 Hilbert–Huang Transform

The Empirical Mode Decomposition (EMD) is first proposed by Dr. Huang in [17]. It is an algorithm for the analysis of multi-component signals that works by breaking them down into a number of amplitude- and frequency-modulated (AM/FM) zero-mean signals. In contrast to conventional decomposition methods, which perform the analysis by projecting the signal into a number of predefined basis vectors, EMD expresses the signal as an expansion of basic functions which are estimated by an iterative procedure called sifting. The essence of EMD is to identify the IMF by their characteristics in timescales in the data empirically. The principle steps of EMD are introduced as follows [17, 18]:

1. Find all the local minima and maxima of the signal $x(t)$;
2. Set up the upper envelope $u_k(t)$ and lower envelope $l_k(t)$ by the B-spline interpolation;
3. Calculate the mean value $m_k(t) = (u_k(t) + l_k(t))/2$;
4. Subtract the $m_k(t)$ from original signal and get the residue $h_k(t) = x_k(t) - m_k(t)$;
5. Repeat the steps from 1 to 4, if the $h_k(t)$ satisfies the conditions of IMF, then extract the $h_k(t)$ and record it as $c_k(t) = h_k(t)$;
6. Determine the IMFs and obtain the residue $r_n(t) = x_n(t) - c_k(t)$;
7. Check whether $r_n(t)$ is a mono-component or not; if not, then return to Step 1 and repeat the iteration process until the $r_n(t)$ only has three extrema.

The flowchart of EMD is displayed in Fig. 2.10.

In Fig. 2.10, there are two loops in the process of EMD. The internal loop is called sifting, which is used to extract the intrinsic mode functions (IMFs); and the external loop is the main iteration, which is implemented to define the numbers of

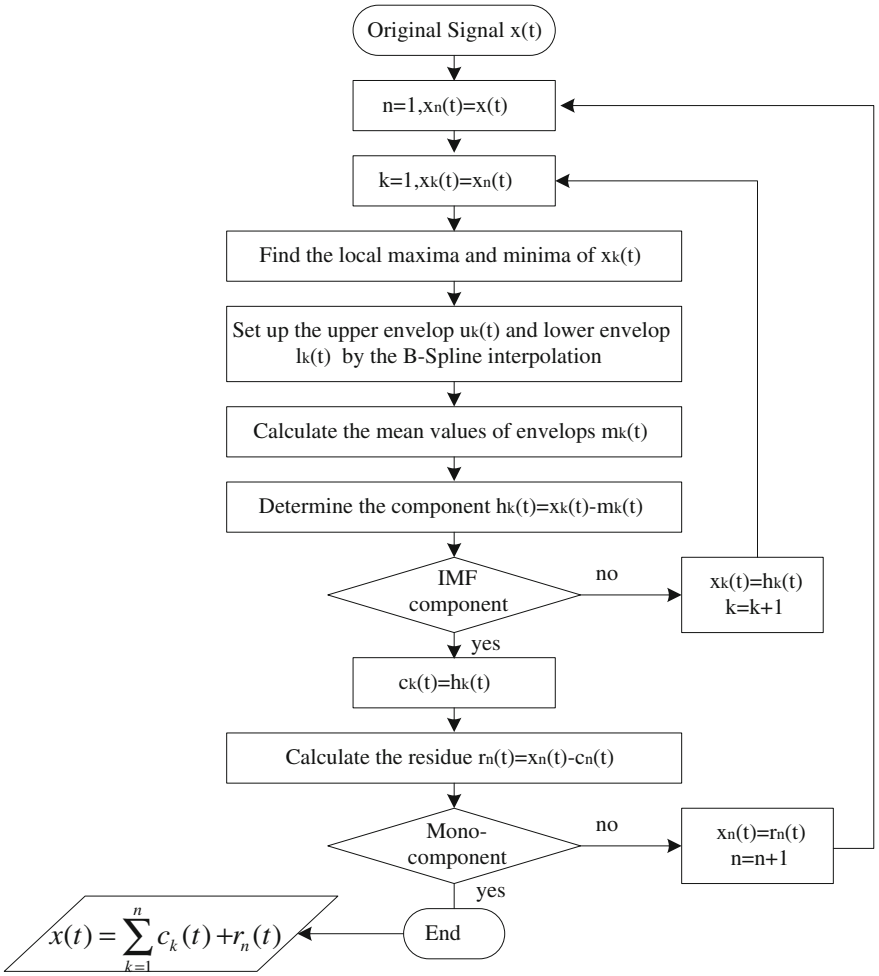

Fig. 2.10 The flowchart of EMD

IMFs and end the process of decomposition. After EMD, the signal can be expressed into two parts [19]:

$$x(t) = \sum_{k=1}^{n} c_k(t) + r_n(t) \tag{2.47}$$

$c_k(t)$ stands for the IMF and n is the numbers of IMF; $r(t)$ indicates the residue of the signal.

From the perspective of sifting process, all the IMFs should be locally orthogonal to each other because IMF is got by subtracting its local mean from the signal.

Obviously, the results are not fully orthogonal because the local mean is not the true value while calculated by the lower and upper envelopes. In [17], the index of orthogonal (IO) and energy leakage are employed to evaluate the orthogonal degree of the EMD. Empirically, in most cases in power system, the energy leakage is small and the IMFs obtained by EMD can be considered near orthogonal to each other.

From the form of analytical function, the conceptions of instantaneous amplitude and envelope of signal have been well accepted. However, the notion of instantaneous frequency is still highly controversial. In [17], it is noticed that there are still considerable defects in defining the instantaneous frequency as follows:

$$f(t) = \frac{1}{2\pi}\frac{\mathrm{d}\varphi(t)}{\mathrm{d}t} \tag{2.48}$$

In (2.48), it is clear that the instantaneous frequency is a single value function of time. The instantaneous frequency is determined by the specific time. Therefore, it can only represent one component named "mono-component." But it is difficult to judge whether a function is "mono-component" or not because there is no precise and strict definition.

From the description above, notion of instantaneous frequency is based on the assumption that there is only one single frequency component at each time instant. Thus, under the condition that $x(t)$ is a multi-component signal, the obtained results are meaningless. A set of synthetic signals is used to illustrate this problem:

$$\begin{cases} x_1 = \sin(1.2\pi t) \\ x_2 = 1.5\mathrm{e}^{-0.1t}\sin(1.5\pi t) \\ x_3 = x_1 + x_2 \end{cases} \tag{2.49}$$

It is clear that x_1 is a pure sine signal, x_2 is an exponential decay signal, and x_3 is a composite signal. At the given time t, x_1 and x_2 have the unique frequency. The value has no any relations with the values at other times. However, the instantaneous frequency of x_3 is meaningless because it is a superposition value. The comparison results are displayed in Fig. 2.11.

Figure 2.11 compares the analytical functions, instantaneous amplitudes, and instantaneous frequencies of three original signals. The main conclusions can be summarized as follows: (1) for the analytical functions, x_1 is a standard circle while there are obvious distortions on the both ends of x_1 and x_2; (2) the instantaneous frequency of x_1 is equivalent to 0.6 Hz at all the time range, the instantaneous amplitude is one constant; (3) for x_2, its frequency is nearly to 0.75 Hz except the both end areas of the signal, these phenomena can also be seen from the instantaneous amplitudes, and it will be discussed in next chapter; and (4) both the amplitude and frequency of x_3 are irregular and insignificant.

In order to get the accurate instantaneous frequency, a new definition of a class of function named intrinsic mode function (IMF) is proposed in [17]. The IMF should satisfy two conditions: (1) the number of extrema and the number of zero crossings must either equal or differ at most by one in the whole data range; (2) at

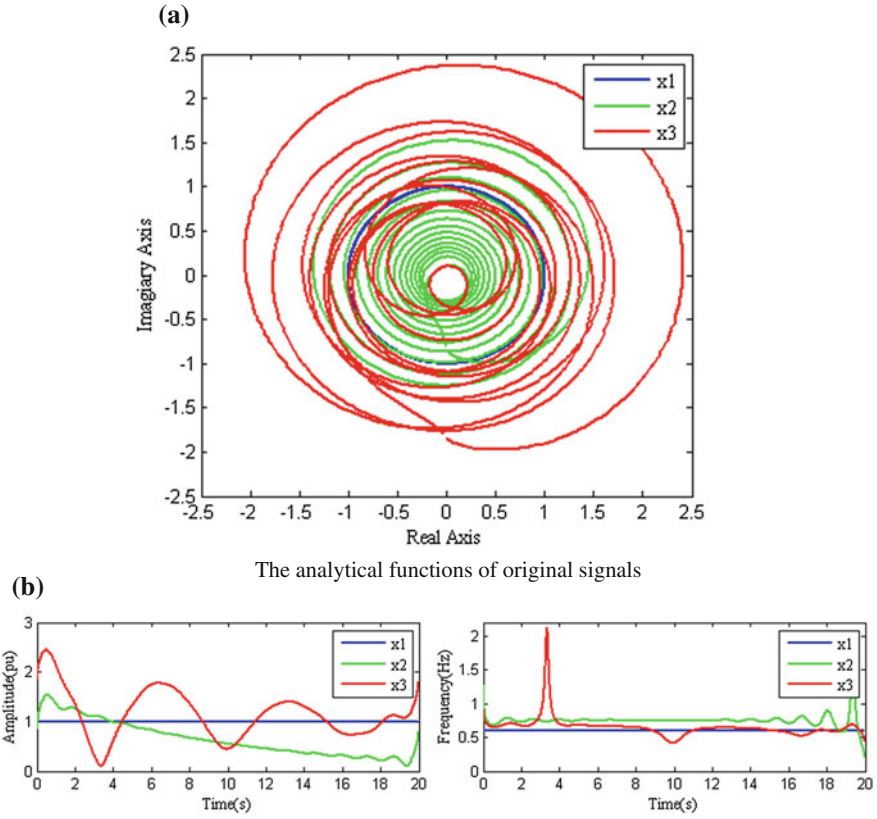

Fig. 2.11 The comparison of instantaneous parameters

any point, the mean value of the upper envelope defined by the local maxima and the lower envelope defined by the local minima is zero.

From the definition of IMF, it is clear that the IMF is adopted because it represents the oscillation mode imbedded in the data. In order to define the instantaneous frequency clearly, the EMD is employed to decompose the single nonlinear signal into the needed IMFs.

Hilbert–Huang Transform

In this section, the analytical function is introduced first. In general, the HT form of a real function $x(t)$ is defined as follows [17, 20]:

$$y(t) = \frac{1}{\pi} P \int_{-\infty}^{+\infty} \frac{x(\tau)}{t-\tau} \mathrm{d}\tau \tag{2.50}$$

where P indicates the Cauchy principal value.

Clearly, the HT form of $x(t)$ is a linear operation. The inverse HT, by means of the original signal $x(t)$ recovered from $y(t)$, is calculated by

$$x(t) = -\frac{1}{\pi} P \int_{-\infty}^{+\infty} \frac{y(\tau)}{t-\tau} \mathrm{d}\tau \tag{2.51}$$

The detailed introduction of HT with the emphasis on its mathematical foundation can be found in [20]. $y(t)$ is interpreted as the convolution of $x(t)$ with the time function $1/\pi t$. Therefore, it gives the emphasis on the local properties of $x(t)$. It is well known that the convolution of two functions in time domain can be transformed into the multiplication of their FFTs in frequency domain. Therefore, HT can also be interpreted as a $\pi/2$ phase shifter, which means the amplitudes of all frequency components in the signal are unchanged while the phases of them are shifted by $\pi/2$.

Comparing the FFT, HT has a number of useful properties for analyzing the LFO signal [20]: (1) $x(t)$ and $y(t)$ have the same magnitude spectrum; (2) the HT form of $y(t)$ is $x(t)$; (3) $x(t)$ and $y(t)$ are orthogonal over the entire time interval; and (4) HT form of $\dot{x}(t)$ is equivalent to the derivative of $y(t)$.

According to the relationship between $x(t)$ and $y(t)$, the form of analytical function is defined as follows:

$$z(t) = x(t) + jy(t) = A(t)\mathrm{e}^{j\phi(t)} \tag{2.52}$$

$$\begin{cases} A(t) = \sqrt{x^2(t) + y^2(t)} \\ \phi(t) = \arctan(y(t)/x(t)) \end{cases} \tag{2.53}$$

where $A(t)$ is the instantaneous amplitude, and $\phi(t)$ is the instantaneous phase.

The analytical signal represents a time-dependent phasor in the complex plane with instantaneous amplitude and phase. Figure 2.12 gives two conceptual representations of the analytical signal.

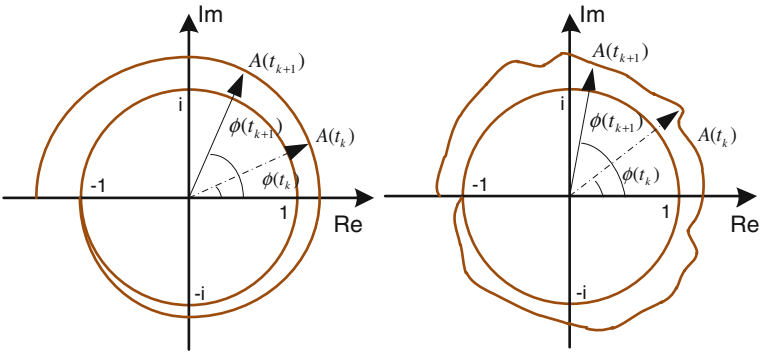

Fig. 2.12 Two conceptual representations of the analytical signal

Theoretically, although many methods have been proposed to define the imaginary parts of the analytical function, the HT is the unique and convenient way to set up the analytical function.

2.4 Summary

This chapter presents the theoretical foundation of LFO. Two techniques are presented to analyze the LFOs, one based on system model and the other based on measured information. Model-based method has been widely utilized to obtain the model of power system to design the controller. The key idea of model-based methods is that the whole system is linearized around a specific operating point. Then the system model is described as the state equations. The eigenvalues, eigenvectors, and participation factors of the state matrix are calculated. The oscillatory parameters including the frequency and damping ratio of each mode are determined by the eigenvalues. While the measurement-based methods has been investigated for extracting model information from measured system responses, most of the methods based on the ensemble measurement matrix can extract the oscillation mode shape or similar results. However, they cannot provide time-varying and nonlinear oscillatory parameters of each single measured signal. Furthermore, the calculated results cannot be directly utilized to estimate the stability of the oscillation mode.

References

1. Rogers G (2000) Power system oscillations. Kluwer Academic Publishers, Norwell. ISBN 0-7923-7712-5
2. DeMello FP, Corcordia C (1969) Concept of synchronous machine stability as affected by excitation control. IEEE Trans Power Appar Syst 88(4):316–329
3. Xu YH, ZH JB (2011) The resonance mechanism low frequency oscillations induced by nonlinear governor system. In: International conference on business management and electronic information (BMEI), 13–15 May 2011
4. Yu YP, Min Y, Chen L et al (2011) The disturbance source identification of forced power system oscillation caused by continuous cyclical load. In: International conference on electric utility deregulation and restructuring and power technologies (DRPT), 6–9 July 2011
5. Seydel R (2009) Practical bifurcation and stability analysis, 3rd edn. Springer, New York. ISBN 978-1-4419-1739-3
6. Wen XY (2005) A novel approach for identification and tracing of oscillatory stability and damping ratio margin boundaries. A Dissertation for PhD degree, Iowa State University
7. Prabha K (2004) Power system stability and control. McGraw-Hill, New York
8. Rogers G (2000) Power system oscillations. Kluwer
9. Klein M, Rogers GJ, Kundur P (1991) A fundamental study of inter-area oscillations. IEEE Trans. Power Syst 6:914–921
10. Kundur P (1993) Power system stability and control. McGraw-Hill, New York

11. Sadikovi'c R (2006) Use of FACTS devices for power flow control and damping of oscillations in power systems. PhD Dissertation, Swiss Federal Institute of Technology Zurich
12. Phadke AG, Thorp JS (2008) Synchronized phasor measurements and their applications. Springer, New York
13. Restrepo JQ (2005) A real-time wide-area control for mitigating small-signal instability in large electric power systems. A Dissertation for PhD degree, Washington State University
14. Trudnowski DJ, Johnson JM, Hauer JF (1998) SIMO system identification from measured ringdowns. In 1998 Proceedings of the American control conference, pp 2968–2972
15. Zemmour AI (2006) The Hilbert-Huang transform for damage detection in plate structures. A Dissertation for PhD degree, Master of Science
16. Turunen J (2011) A wavelet-based method for estimating damping in power systems. Doctoral Dissertations, Aalto University Publication Series
17. Huang NE, Shen Z, Long SR et al (1998) The empirical mode decomposition and the Hilbert spectrum for nonlinear and non-stationary time series analysis. Proc R Soc Lond A 454:903–995
18. Messina AR (2009) Inter-area oscillations in power systems: a nonlinear and non-stationary perspective. Springer, Berlin. ISBN 978-0-387-89529-1
19. Yuan ZY, Tao X, Zhang Y C et al (2010) Inter-area oscillation analysis using wide area voltage angle measurements from FNET. IEEE power and energy society general meeting 25–29 July 2010
20. Li W, Robert MG, Dong J Y et al (2009) Wide area synchronized measurements and inter-area oscillation study. IEEE/PES power systems conference and exposition (PSCE), 15–18 Mar 2009

http://www.springer.com/978-3-662-48625-2

Interconnected Power Systems
Wide-Area Dynamic Monitoring and Control Applications
Li, Y.; Yang, D.; Liu, F.; Cao, Y.; Rehtanz, C.
2016, XV, 223 p. 143 illus., Hardcover
ISBN: 978-3-662-48625-2